博 士 論 文

# Assessment of bone forming ability of apatite-coated collagen scaffold prepared by a precursor-assisted biomimetic process
# (前駆体を利用した生体模倣プロセスにより作製されたアパタイト被覆コラーゲンスキャフォールドの骨形成能の評価)

令和２年３月申請

北海道大学

大学院歯学研究科口腔医学専攻

金　本　佑　生　実

# Assessment of bone forming ability of apatite-coated collagen scaffold prepared by a precursor-assisted biomimetic process

Yukimi KANEMOTO

**Institutions**

Department of Periodontology and Endodontology, Graduate School of Dental Medicine, Hokkaido University

N13, W7, Kita-ku, Sapporo, 060-8586, Japan.

**Key words**

Atelocollagen scaffold, biomimetic mineralization, bone tissue engineering, histological measurement, low-crystalline apatite, MC3T3-E1 cells, rat, RT-PCR

**Abstract**

Three-dimensional collagen scaffold (CS) coated with low-crystalline apatite via a precursor-assisted biomimetic process reportedly enhanced cellular responses and blood vessels formation. In this study, Osteogenic properties of apatite-coated collagen scaffold (Ap-CS) were examined by in vitro cell culture tests and rat bone forming tests.

After oxygen plasma treatment, CS was alternately dipped in $CaCl_2$ and $K_2HPO_4 \cdot 3H_2O$ solutions to be pre-coated with CaP. Subsequently, the CS was immersed in a supersaturated CaP solution to be coated with apatite. The resulting Ap-CS was characterized by observation using a scanning electron microscope (SEM), and assessments of water absorption, Ca ion release, protein adsorption and enzyme resistance. Cytotoxic tests and real-time RT-PCR were carried out using MC3T3-E1 osteoblastic

cells. In addition, bone forming ability of Ap-CS was histologically evaluated after implantation onto the rat skull.

SEM observation revealed that the surface of Ap-CS was covered with nanostructured deposition. It is considered that a layer of low-crystalline apatite was formed on CS through the precursor-assisted biomimetic process as reported previously. Ap-CS significantly increased water adsorption, Ca ion release, cationic protein adsorption and resistance to collagenase enzymatic effect, compared with CS. In cell culture studies, Ap-CS decreased the cell proliferation, however, the expression of bone formation markers, such as bone sialoprotein and osteocalcin, was promoted compared with CS. Ap-CS significantly promoted new bone augmentation of rat skull. Furthermore, residual scaffold was slight when compared to CS. In conclusion, Ap-CS exhibited bone forming activity to be beneficial for bone tissue engineering therapy.

## 1. Introduction

Periodontal disease frequently causes the destruction of the alveolar bone, related to tooth supporting system, through the inflammatory responses. The purpose of bone tissue engineering is to regenerate lost bone tissue using three elements[1)], cells[2-4)], growth factors[5-8)], and scaffolds[9-11)]. Scaffolds create a space for tissue regeneration and play an important role in retention of growth and nutrition factors, cell proliferation and differentiation, vascular network construction and extracellular matrix secretion[12)]. In general, sintered calcium phosphates (CaPs), such as hydroxyapatite (HA) and β-tricalcium phosphate (β-TCP), have been used for osteoconductive scaffolds, due to their compositional similarity to the human bone minerals[13-14)]. Bioceramics have the biocompatibility and the osteoconductivity[15-16)], however, have the disadvantage

regarding low biodegradability. HA is rarely degraded after implantation and remained in the body as the residue for a long term[17-19]. In addition, β-TCP reportedly remained in the body for over a half year, although β-TCP is known to be biodegradable[20-21]. Because bone defect created by periodontal disease is located close to oral cavity, scaffold should rapidly biodegrade while supporting bone regeneration, to reduce infection risk.

Natural bone shows a hierarchical structure including apatite crystals deposited on a nano-network of collagen matrix[22]. Therefore, it is expected that a similar nanocomposite, i.e., apatite-coated collagen network, would be beneficial as a scaffold for bone regeneration[23]. It is known that low-crystalline apatite can be coated on a substrate using an acellular supersaturated CaP solution as a coating medium, like in vivo bone apatite formation. The thus-formed low-crystalline apatite exhibits good biocompatibility and osteoconductivity, as well as the higher biodegradability compared to sintered HA ceramics[24]. The low-crystalline apatite coating process using supersaturated CaP solutions (biomimetic process) is a mild liquid phase method that can be carried out under normal temperature and pressure, and applicable to low-melting-point materials including organic polymer collagen. These are noteworthy advantages of the biomimetic process over conventional CaP coating processes such as plasma spraying[25-26], pulse laser deposition[27-28] and sputtering methods[29-30]. Oyane et al. previously developed a precursor-assisted biomimetic process as a relatively simple biomimetic process[31]. In the process, a substrate is pre-coated with amorphous CaP as the apatite precursor through the alternate dipping treatment in Ca and P solutions, and then immersed in a supersaturated CaP solution for low-crystalline apatite coating. They succeeded in apatite coating on various materials, including porous blocks[32], fibers[33] and sponges[34] by the precursor-assisted biomimetic process.

Recently, Joseph et al. fabricated three-dimensional collagen scaffold (CS) coated with low-crystalline apatite by the precursor-assisted biomimetic process[35]. The apatite-coated collagen scaffold (Ap-CS) promoted cell and blood vessel in-growth into the scaffold compared to the uncoated CS in rat subcutaneous tissue[35]. However, no report has shown the bone forming ability of the Ap-CS made by the precursor-assisted biomimetic process. The purpose of this study was to perform in-depth characterization of the Ap-CS. In vitro cell culture tests were carried out to elucidate the osteogenic properties of the Ap-CS. In addition, bone forming ability of the Ap-CS was histologically examined after implantation onto the rat skull.

## 2. Material and Methods

### 2.1. Fabrication of the Ap-CS

An Ap-CS was fabricated as described previously[35]. A calf atelocollagen-based CS (Terudermis®, Olympus Terumo Biomaterials Corp., Tokyo, Japan) was cut into cuboidal pieces (6 mm × 6 mm × 3 mm, Figure 1, left) and treated with oxygen plasma to increase hydrophilicity of the surface. The plasma treatment was carried out using an $O_2$ gas (99.9995%, Takachiho Chemical Industrial Co., Ltd., Tokyo, Japan) at a plasma power density of 0.1 W/cm$^2$ and a pressure of 30 Pa under an electric field operating at 13.56 MHz for 30 s using a compact ion etcher (FA-1, Samco Inc., Kyoto, Japan). After plasma treatment, scaffolds (3 pieces) were immersed in 30 mL of a 200 mM $CaCl_2$ solution, washed with 30 mL of ultrapure water, and immersed in 30 mL of a 200 mM $K_2HPO_4{\cdot}3H_2O$ solution to be pre-coated with CaP (seeds for apatite growth). We employed a vacuum degassing system to fill and replace solutions throughout the interconnected porous structure of the CS as detailed in our previous report[35].

The CS removed from the 200 mM $K_2HPO_4 \cdot 3H_2O$ solution was rinsed with a supersaturated CaP solution (CP solution), and subsequently immersed in 30 mL of a CP solution for 48 h at 25°C to grow CaP seeds into an apatite coating layer. The CP solution was prepared by dissolving reagent-grade NaCl (final concentration = 142 mM), $K_2HPO_4 \cdot 3H_2O$ (1.50 mM), HCl (40 mM), and $CaCl_2$ (3.75 mM) in ultrapure water. The pH of the solution was adjusted to a final value of 7.4 at 25°C using tris(hydroxymethyl)aminomethane (50 mM) and the required amount of 1 M HCl. All the reagents used for the solution preparation were purchased from Nacalai Tesque, Inc., Kyoto, Japan. After 48 h of immersion in the CP solution, the scaffold was washed with ultrapure water and freeze-dried using a freeze drier (model DC41, Yamato Scientific Co., Ltd., Japan and FDS-1000, Tokyo Rikakikai Co., Ltd., Tokyo, Japan) to finally obtain Ap-CS (Figure 1, right).

### 2.2. SEM observation

The surface structures of Ap-CS and CS were characterized using scanning electron microscopy (SEM, S-4000; Hitachi, Tokyo, Japan) with an accelerating voltage of 10 kV after coating with a thin layer of Pt-Pd.

### 2.3. Water absorption capacity

Water absorption capacity of scaffold was assessed as described previously[36]. CS and Ap-CS were weighed and immersed in sterile distilled water (Otsuka Pharmaceutical Co. Ltd., Tokyo, Japan) for 30 m at room temperature. After wiping excess water from the scaffold using whatman filter paper (GE Healthcare Japan Co., Ltd., Japan), scaffold was weighed for absorbed water.

### 2.4. Calcium ion releasing test

Calcium ion release from the CS and Ap-CS was assessed using a calcium test kit (calciumE-test; FUJIFILM Wako Pure Chemical Corp., Osaka, Japan). CS and Ap-CS were immersed in phosphate-buffered saline (PBS, FUJIFILM Wako Pure Chemical Corp.) at 37°C for 7 days. The calcium content in the supernatant was measured by spectrophotometer (U-1100; Hitachi, Ltd., Tokyo, Japan) at 610 nm.

### 2.5. Protein adsorption test

To detect the ability of anionic and cationic protein adsorption of the scaffold, 100 μL of distilled water supplemented with 50 μg bovine serum albumin (FUJIFILM Wako Pure Chemical Corp.) or 50 μg lysozyme hydrochloride (from egg white; FUJIFILM Wako Pure Chemical Corp.) was prepared and CS and Ap-CS were immersed under a vacuum condition. Subsequently, CS and Ap-CS were immersed into 1.0 mL of deionized distilled water for 10 m. After stirring well, the protein content of the supernatant was measured with spectrophotometer at 610 nm using a total protein kit (Micro Lowry, Peterson's Modification; Sigma-Aldrich Co., St Louis, MO, USA). Then, the amount of albumin and lysozyme adsorbed onto the scaffold were calculated.

### 2.6. Enzyme degradation test

To detect the collagenase resistance of the scaffold, CS and Ap-CS were weighed and then immersed into 1 mL of PBS containing 1% collagenase type I (0.1 mg / mL; FUJIFILM Wako Pure Chemical Corp.) for 3 h at 37°C. After that, scaffold was dehydrated into absolute ethanol, air-dried and weighed as the residual amount of scaffold.

### 2.7. Cyto-compatibility assessments

Mouse osteoblastic MC3T3-E1 cells ($5\times10^4$; RIKEN BioResource Center, Tsukuba, Japan) were seeded on CS and Ap-CS and cultured in humidified 5% $CO_2$ at 37°C in 48-well plates, using a minimum essential medium (MEM) (alpha-GlutaMAX™-I; Thermo Fisher Scientific Inc., Waltham, MA, USA) supplemented with 10% fetal bovine serum (FBS) (Qualified; Thermo Fisher Scientific Inc.) and 1% antibiotics (penicillin/streptomycin; Thermo Fisher Scientific Inc.). The cyto-compatibility of scaffold was assessed at 1, 3, 5 and 7 days of culture using assay kits of water-soluble tetrazolium salt (WST)-8 (Cell Counting Kit-8, Dojindo Laboratories, Mashiki, Japan) and a lactate dehydrogenase (LDH, Cytotoxicity LDH Assay Kit-WST, Dojindo Laboratories) using a microplate reader (ETY-300, Toyo Sokki Co., Ltd., Japan) at 450 nm and 490 nm, respectively.

For the cell adhesion assay, 24 h cultured CS and Ap-CS inoculated with MC3T3-E1 cells ($7\times10^3$) was washed with PBS and fixed with 3.5% formaldehyde. A staining solution was prepared by dissolving phalloidin (1.5 μg, Actistain 555 Fluorescent Phalloidin, Cytoskeleton Inc., Denver, CO, USA) and 4’ ,6-diamidino-2-phenylindole (2 μg, Dojindo Laboratories) in 500 μL of a bovine serum albumin (BSA, 7.5% w/v Albumin Dulbecco’s-PBS (−) Solution from bovine serum, FUJIFILM Wako Pure Chemical Corp.). After immersing in this solution at 4°C overnight to stain the cultured cells, the scaffolds were washed with PBS and observed with a fluorescence microscope (Biorevo BZ-9000, Keyence Corp., Osaka, Japan). In addition, MC3T3-E1 cells ($2\times10^3$) on CS and Ap-CS after 24 h incubation were stained with the LIVE/DEAD Viability/Cytotoxicity Kit for mammalian cells (Thermo Fisher Scientific), following the manufacturer’s

instructions. Live cells were stained with calcein acetoxymethyl to create green fluorescence, and cells with compromised membranes were stained with ethidium homodimer-1 to create red fluorescence. Stained samples were examined using a fluorescence microscope.

### 2.8. Real-time reverse transcription-polymerase chain reaction (RT-PCR) assays

MC3T3-E1 cells ($1\times10^6$) were seeded on CS and Ap-CS and cultured in humidified 5% $CO_2$ at 37°C in 48-well plates, using MEM supplemented with 10% FBS and 1% antibiotics. The cultures were incubated at 37°C with 5% $CO_2$. MEM exchange performed every 2 days. After 14 days, total RNA was extracted using Trizol (Invitrogen, Carlsbad, CA, USA) according to the manufacturer's instructions. Reverse transcription was conducted with 1 μg of RNA to obtain cDNA. The cDNA was amplified by Rever Tra Ace-α FSK-101 (Toyobo, Osaka, Japan). Primers (Applied Biosystems, Carlsbad, CA, USA) for the following genes were used: Ibsp (Mm00492555_m1), Bglap1 (Mm03413826_m1) and glyceraldehyde-3-phosphate dehydrogenase (GAPDH, Mm99999915_g1). Real-time RT-PCR was performed using the ABI Prism 7300 sequence detection system (Applied Biosystems). Data obtained for each sample were standardized against the expression of GAPDH and were calculated using the 2-ΔΔCt method[37-38].

### 2.9. Animal procedure

In vivo experiments using rats were performed in accordance with the institutional animal use and care regulations of Hokkaido University (approval number 16-29) and approved by the Animal Research Committee of Hokkaido University. Sixteen 10-week-

old male Wistar rats weighing 190–210 g were used in this study. Surgical operations were performed under general anesthesia by intraperitoneal injection of medetomidine hydrochloride (0.15 mg/mL, Domitor; Nippon Zenyaku Kogyo Co., Ltd., Koriyama, Japan), Midazolam (2 mg/mL, Dormicum; Astellas Pharma Inc., Tokyo, Ja-pan), butorphanol tartrate (2.5 mg/mL, Vetorphale; Meiji Seika Pharma Co., Ltd., Tokyo, Japan) and local injection of 2% lidocaine hydrochloride with 1:80,000 epinephrine (Xylocaine Cartridge for Dental Use; Dentsply Sirona K.K., Tokyo, Japan).

After the rat skull was exposed, 4 $mm^2$ decortication was created by Maillefer steel round bur (Dentsply Sirona K.K., Tokyo, Japan) under irrigation with saline (Otsuka Pharmaceutical Factory, Inc., Tokushima, Japan). Subsequently, CS or Ap-CS was placed onto the decortication area and skin was sutured (BioFit-D 4-0; Washiesu medical Co., Ltd., Tokyo, Japan), and an ointment containing tetracycline hydrochloride (achromycin ointment; POLA Pharma Inc., Tokyo, Japan) was applied to the wound.

### 2.10. Histological procedure

At 10 days after surgery, 4 rats were perfused via the aorta with 4% formaldehyde under general anesthesia. The rat skull including implanted scaffold were pre-fixed by 4% formaldehyde for 24 h, dipped in 30% sucrose solution and embedded in optimal cutting temperature compound (Sakura Finetek Inc., Tokyo, Japan). After frozen in liquid nitrogen, approximately 16 μm thick sections were prepared and placed on poly-l-lysine-coated glass slides. After pretreatment with 0.3% Triton X-100 and normal donkey serum, the sections were incubated overnight with the following primary antibodies: mouse anti-CD68 (1:100 in dilution; Bio-Rad Laboratories Inc., Hercules, CA, USA), mouse anti-CD163 (1:100 in dilution; Bio-Rad Laboratories Inc.), rabbit anti-Sp7/Osterix antibody –

ChIP Grade (1:400 in dilution; Abcam plc, Cambridge, UK). The antigen–antibody reaction sites were detected by incubation with Cy3-labeled anti-mouse IgG (Jackson ImmunoResearch Inc., West Grove, PA, USA). Nuclear was stained by TOTO3 (Thermo Fisher Scientific Inc.). The sections were observed under a fluorescence microscope. The sections incubated with normal mouse serum instead of respective primary antibody were used as negative controls.

After 35 days of surgery, 10 rats were euthanized by overdose of pentobarbital sodium (2 mL / kg). Samples of rat skull were fixed in 10% buffered formalin, decalcified with 10% ethylenediaminetetraacetic acid, and embedded in paraffin. After thin sectioning (thickness 6μm), the sections were stained with hematoxylin and eosin (HE) and observed with light microscope. Histomorphometric measurements of the new bone height, new bone area, and residual scaffold area was performed using software (Image J 1.41; National Institutes of Health, Bethesda, MD, USA). In addition, 2 rats implanted with Ap-CS was selected for immunostaining, using primary antibody; anti-Sp7/Osterix, rabbit anti-Osteopontin (OPN; 1:800 in dilution; Abcam plc, Cambridge, UK), mouse anti-α-smooth muscle actin (ASMA; 1:1,600 in dilution, clone 1A4; Sigma-Aldrich Co., St Louis, MO, USA) and mouse anti-rat endothelial cell antigen-1 (RECA-1; 1:1,000 in dilution; AbD Serotec, Kidlington, UK), in the same procedure as mentioned above.

### 2.11. Statistical Analysis

Each parameter was calculated for means and standard deviation. Differences between groups were analyzed using Student‘s t-test. Results for which $P < 0.05$ were regarded as statistically significant. All statistical procedures were done using SPSS 11.0 (IBM Corporation, Armonk, NY, USA).

## 3. Results

### 3.1. Characterization of scaffolds

The SEM images of the surfaces of CS and Ap-CS are shown in Figure 2. As shown in CS in lower-magnification, CS was constructed with filament- and sheet-like collagen struts and possessed a porous structure. Higher magnification image of sheet-like collagen in CS showed a smooth surface. In contrast, Ap-CS showed nanostructured deposition on its porous surface. This nanostructured deposition should be low-crystalline apatite consisting of Ca and P, according to the previous results of energy dispersive X-ray spectroscopy and X-ray diffraction analysis.[35)]

The water absorption of CS and Ap-CS was 60.0 ± 4.0 and 98.3 ± 5.9 mg, respectively. Amount of water in Ap-CS indicated significantly 1.6-fold increase compared with CS ($P<0.01$, Figure 3A). Calcium ion release from Ap-CS was 0.66 ± 0.15 mg, however, it was not detected from CS ($P<0.01$, Figure 3B). In protein adsorption test, amounts of adsorbed anionic albumin and cationic lysozyme were 14.7 ± 3.3 and 32.4 ± 4.5 μg in CS and 17.9 ± 4.5 and 42.5 ± 6.2 μg in Ap-CS, respectively. Adsorption of lysozyme to Ap-CS was significantly higher than that of CS ($P<0.05$, Figure 3C). In enzymatic degradation tests, the weigh before and after collagenase treatment was 4.39 ± 0.43 and 0.76 ± 0.13 mg in CS, and 7.72 ± 1.49 and 6.04 ± 1.21 mg in Ap-CS, respectively. The rate of weight decreasing of CS and Ap-CS was 82.8 ± 1.8 and 21.9 ± 2.7 %, respectively. Decrease of Ap-CS was significantly less than that of CS ($P<0.01$, Figure 3D).

### 3.2. Cyto-compatibility assessments of scaffolds

The fluorescence images of f-actin and live/dead staining were shown in Figure 4A. F-actin staining revealed that cell elongation related to expression of actin fiber were observed on both CS and Ap-CS (stained in red). In the assessment of LIVE/DEAD BacLight staining, osteoblastic MC3T3-E1 cells on CS and Ap-CS were mostly stained in green, indicating live cells.

The results of WST-8 and LDH assays are presented in Figure 4B and C. In WST-8 assay, there was no significant difference of WST-8 activity between CS and Ap-CS at 1 day. However, although WST-8 activity of CS increased until 7 days, WST-8 activity of Ap-CS at 3, 5, 7 days was low values and equivalent to activity of 1 day, and significantly lower compared with CS ($P<0.05$). In LDH activity assay, CS and Ap-CS showed equivalent activity at 1 and 7 days. Ap-CS at 3 and 5 days had a high LDH activity, showing a significant difference compared to the CS ($P<0.05$).

### 3.3. Real-time RT-PCR assessments

Measurements of amplified cDNA by real-time RT-PCR demonstrated that Ap-CS increased the expression of osseous markers; bone sialoprotein (BSP) and osteocalcin (OCN), of MC3T3-E1 cells. Significant difference was found between CS and Ap-CS ($P<0.05$, Figure 5).

### 3.4. In vivo assessments at 10 days after implantation

In the examination of the implantation of CS and Ap-CS onto rat skull, CD68, CD163 and SP7 immunostaining (stained in red) was carried out (Figure 6). Macrophage expressing CD68 was frequently showed into and around both CS and Ap-CS (white arrowheads). CD163 positive macrophage rarely observed in the image of CS, however,

Ap-CS positively showed CD163 positive cells at the inner region of implanted sample (red arrowheads). Osteoblastic cells expressing Sp7 were found at the surface region of skull bone covered with implanted CS. However, Ap-CS applied sample revealed that Sp7 positive cells frequently found at the inner region of Ap-CS, as well as the surface region of skull bone (yellow arrowheads).

### 3.5. In vivo assessments at 35 days after implantation

HE stained images at 35days after implantation of CS (Figure 7A-C) frequently showed the residue of CS on the cranial bone. Residue was composed of few cells and collagen substance (Figure 7B). Newly formed bone continuous with pre-existing bone was slightly found to repair the bone defect (Figure 7C). In contrast, new bone was remarkably formed after implantation of Ap-CS (Figure 7D-F). Bone tissue was augmented from pre-existing skull bone and included bone marrow structure (white arrowheads). Osteoblastic cells were positioned along with surface of new bone (black arrows) (Figure 7E and F) and were immunohistochemically stained with SP7 and OPN (white arrowheads in figure 8). The connective tissue covering new bone was cell-rich (Figure 7E) and frequently included many blood vessel-like structures immunoexpressed with ASMA and RECA-1(yellow arrowheads in figure 8).

Histometric measurements (Figure 9) revealed that new bone area and height of CS and Ap-CS were 0.16 ± 0.01 $mm^2$, 0.12 ± 0.04 mm, and 0.74 ± 0.50 $mm^2$, 0.34 ± 0.10 mm, respectively. Parameters of bone formation of Ap-CS were significantly greater than CS ($P<0.05$). The residual scaffold area of CS and Ap-CS was 0.34 ± 0.16 and 0.09 ± 0.05 $mm^2$, respectively. The residual scaffold area was significantly decreased in Ap-CS compared with CS ($P<0.01$).

## 4. Discussion

Cell culture examination revealed that cell behaviors, such as elongation and spreading of osteoblastic MC3T3-E1 cells, were similar in both CS and Ap-CS. In addition, attached cells on Ap-CS mostly stained in green (alive) in live/dead staining. Accordingly, Ap-CS likely exhibited good cell affinity as the scaffold. However, WST-8 activity of cultured Ap-CS was consistently low compared with CS, excepting for assay at 1 day. It was considered that MC3T3-E1 cells inoculated on Ap-CS did not proliferate on its surface of the scaffold through experimental periods, in contrast to CS. From the evidence, we speculated that Ap-CS exhibited the differentiation-inducing activity. Bioactive material including HA consistently and strongly stimulated the osteogenic differentiation of cells instead of proliferation, to lead toward bone formation[39-40]. In addition, ion releasing assessment in present study showed the evidence of Ca ion release from Ap-CS, in contrast to CS (no release of Ca ion). Maeno et al. reported that application of high concentration of Ca to cells dose-dependently suppressed cell proliferation[41]. Lee et al. also revealed that relatively high concentration of Ca could enhance osteogenic differentiation of mesenchymal stem cells[42]. The enhancement of osseous differentiation in the present study is evident from the significant increased expression of osteogenic markers BSP and OCN in MC3T3-E1 cells cultured on Ap-CS. BSP and OCN are the non-collagenous proteins which stimulate the osteogenic differentiation[43-44]. In addition, we confirmed in this study that Ap-CS remarkably augmented new bone formation after implantation in the rat skull. Therefore, it is likely that Ap-CS stimulates osteogenic differentiation via Ca ions released from the created low-crystalline apatite and consequently promotes the bone formation *in vivo*.

Immunohistochemical staining of Ap-CS reveals cell-ingrowth into the scaffold after 10-days of implantation. CD163-positive macrophages (M2 macrophages) were frequently found in the Ap-CS when compared with CS, in contrast to CD68-positive pan-macrophages recognized in both CS and Ap-CS. M2 macrophages are associated with immunosuppression and enhance tissue repair, remodeling, and subsequent wound healing[45]. In addition, osteoinductive cytokines, BMP-2, VEGF and TGF-β are secreted by M2 macrophages[46]. Immuno-interaction between biomaterial and macrophages via ion-release was described previously[47]. Sugimoto et al. reported that Ca stimulated the chemotaxis reaction of monocyte associated with proliferation and differentiation of osteoblasts[48]. Actually, well-ingrowth of Sp7-positive osteoblast progenitors into Ap-CS was observed in this study. Releasing of Ca ion from low-crystalline apatite of Ap-CS may play a key role in macrophage behaviors and promoting bone tissue formation.

From the evidences of SEM images, EDX and XRD analysis[35], nano-structural low-crystalline apatite was formed to cover the surface of CS. From the result of enzyme degradation test, Ap-CS exhibited the collagenase resistance. Hence, most part of collagen strut of scaffold was likely covered with low-crystalline apatite through biomimetic process. It was reported that the material surface properties including electrical charge and hydrophilicity, affect the ability of cell adhesion and its bioactivity[49-51]. In the water absorption test, Ap-CS significantly absorbed more water compared with untreated CS, suggesting that the surface of Ap-CS acquired hydrophilic surface. Reportedly, hydrophilic surfaces of substrates promoted the cell attachment with expression of adhesion protein, vinculin[49]. Some reports explained the biomaterial for drug delivery systems exhibited the bioadhesive capability via electrostatic potential[52]. In the present study, to examine the electrostatic potential capability of Ap-CS, protein

adhesion test was carried out using anionic and cationic proteins. Since albumin charge negatively and lysozyme charge positively, surface charge of the target is speculated by the adsorption behavior of the target to these proteins[15]. In this work, value of albumin adsorption was equivalent between CS and Ap-CS, however, Ap-CS significantly adsorbed lysozyme compared with CS. Accordingly, it was considered that Ap-CS could store proteins, due to surface negative surface charge by precursor-assisted biomimetic process. These properties may promote the regenerative activity of scaffold.

In vivo study revealed that Ap-CS significantly augmented the skull bone with cell rich connective tissue. ASMA-positive vascular smooth muscle cells, and RECA-1-positive endothelial cells associated with blood vessel were frequently found in the connective tissue around the newly formed bone. It is likely that angiogenesis was frequently evoked in the regenerative space. We speculated that Ap-CS stimulated angiogenesis to provide oxygen and nutrition for bone formation and scaffold replacement. Scaffold for periodontal regeneration should possess the property of rapid replacement into the tissue. After implantation of Ap-CS, residue of scaffold was less compared to implantation of CS, suggesting that Ap-CS was degraded to simultaneously create the bone tissue. The early replacement of Ap-CS into tissue may be acquired from low-crystalline apatite, degradable collagen and cell-ingrowth effect and hence, Ap-CS is beneficial for the periodontal regenerative therapy to avoid the postoperative infection.

**5. Conclusion**

This study evaluated the cyto-compatible and osteogenic properties of Ap-CS fabricated by the precursor-assisted biomimetic process. Ap-CS exhibited the ability of Ca ion release, cyto-compatibility and promoting the osteogenic differentiation of

osteoblastic cells. In rat experiments, Ap-CS showed significant bone formation and well-degradation when compared with CS. Therefore, Ap-CS exhibited bone forming activity and will be beneficial for bone tissue engineering therapy.

## 6. Conflicts of interest

The authors have no conflict of interest to declare.

## 7. Acknowledgments

The authors acknowledge Hirofumi Miyaji, Erika Nishida, Saori Miyata, Kayoko Mayumi and Tsutomu Sugaya (Department of Periodontology and Endodontology, Faculty of Dental Medicine, Hokkaido University), Tsukasa Akasaka (Department of Biomedical, Dental Materials and Engineering, Faculty of Dental Medicine, Hokkaido University), Toshihiko Iwanaga (Department of Histology and Cytology, Faculty of Medicine, Hokkaido University), A. Joseph Nathanael, Syama Santhakumar and Ayako Oyane (Nanomaterials Research Institute, National Institute of Advanced Industrial Science and Technology (AIST)) for their technical assistance. This work was supported by JSPS KAKENHI (16K11822 and 18F18106).

## 8. References


1) O'Keefe RJ, Mao J : Bone tissue engineering and regeneration: from discovery to the clinic - an overview. Tissue Eng Part B Rev, 17(6) : 389-392, 2011.

2) Stoppato M, Stevens HY, Carletti E, Migliaresi C, Motta A, Guldberg RE : Influence of scaffold properties on the interrelationship between human bone marrow derived stromal cells and endothelial cells in pro-osteogenic conditions. Acta Biomater, 25 : 16-23, 2015.

3) Zhang R, Lee P, Lui VC, Chen Y, Liu X, Lok CN, To M, Yeung KW, Wong KK : Silver nanoparticles promote osteogenesis of mesenchymal stem cells and improve bone fracture healing in osteogenesis mechanism mouse model. Nanomedicine, 11(8) : 1949-1959, 2015.

4) Fawzy El-Sayed KM, Mekhemar MK, Beck-Broichsitter BE, Bähr T, Hegab M, Receveur J, Heneweer C, Becker ST, Wiltfang J, Dörfer CE : Periodontal regeneration employing gingival margin-derived stem/progenitor cells in conjunction with IL-1ra-hydrogel synthetic extracellular matrix. J Clin Periodontol, 42(5) : 448-457, 2015.

5) Chang CC, Tsai YH, Liu Y, Lin SY, Liang YC : Calcium containing crystals enhance receptor activator of nuclear factor κB ligand/macrophage colony-stimulating factor-mediated osteoclastogenesis via extracellular-signal-regulated kinase and p38 pathways. Rheumatology (Oxford), 54(10) : 1913-1922, 2015.

6) Carreira AC, Zambuzzi WF, Rossi MC, Filho RA, Sogayar MC, Granjeiro JM : Bone morphogenetic proteins: Promising molecules for bone healing, bioengineering, and regenerative medicine. Vitam Horm, 99 : 293-322, 2015.

7) Tian J, Qi W, Zhang Y, Glogauer M, Wang Y, Lai Z, Jiang H : Bioaggregate inhibits osteoclast differentiation, fusion, and bone resorption in vitro. J Endod, 41(9) : 1500-

1506, 2015.

8) Carrel JP, Wiskott A, Moussa M, Rieder P, Scherrer S, Durual S : A 3D printed TCP/HA structure as a new osteoconductive scaffold for vertical bone augmentation. Clin Oral Implants Res, 27(1) : 55-62, 2016.

9) Yoshida T, Miyaji H, Otani K, Inoue K, Nakane K, Nishimura H, Ibara A, Shimada A, Ogawa K, Nishida E, Sugaya T, Sun L, Fugetsu B, Kawanami M : Bone augmentation using a highly porous PLGA/β-TCP scaffold containing fibroblast growth factor-2. J Periodontal Res, 50(2) : 265-273, 2015.

10) Kosen Y, Miyaji Y, Kato A, Sugaya T, Kawanami M : Application of collagen hydrogel/sponge scaffold facilitates periodontal wound healing in class II furcation defects in beagle dogs. J Periodontal Res, 47(5) : 626-634, 2012.

11) Niu CC, Lin SS, Chen WJ, Liu SJ, Chen LH, Yang CY, Wang CJ, Yuan LJ, Chen PH, Cheng HY : Benefits of biphasic calcium phosphate hybrid scaffold-driven osteogenic differentiation of mesenchymal stem cells through upregulated leptin receptor expression. J Orthop Surg Res, 10 : 1-10, 2015.

12) Min Z, Shichang Z, Chen X, Yufang Z, Changqing Z : 3D-printed dimethyloxallyl glycine delivery scaffolds to improve angiogenesis and osteogenesis. Biomater Sci, 3(8) : 1236-1244, 2015.

13) Murakami S, Miyaji H, Nishida E, Kawamoto K, Miyata S, Takita H, Akasaka T, Fugetsu B, Iwanaga T, Hongo H, Amizuka N, Sugaya T, Kawanami M : Dose effects of beta-tricalcium phosphate nanoparticles on biocompatibility and bone conductive ability of three-dimensional collagen scaffolds. Dent Mater J, 36(5) : 573-583, 2017.

14) Eftekhari H, Farahpour MR, Rabiee SM : Histopathological evaluation of potential impact of β-tricalcium phosphate (HA+ β-TCP) granules on healing of segmental

femur bone defect. Bratisl Lek Listy, 116(1) : 30-34, 2015.

15) Ogawa K, Miyaji H, Kato A, Kosen Y, Momose T, Yoshida T, Nishida E, Miyata S, Murakami S, Takita H, Fugetsu B, Sugaya T, Kawanami M : Periodontal tissue engineering by nano beta-tricalcium phosphate scaffold and fibroblast growth factor-2 in one-wall infrabony defects of dogs. J Periodontal Res, 51(6) : 758-767, 2016.

16) Carfì Pavia F, Conoscenti G, Greco S, La Carrubba V, Ghersi G, Brucato V : Preparation, characterization and in vitro test of composites poly-lactic acid/hydroxyapatite scaffolds for bone tissue engineering. Int J Biol Macromol, 119 : 945-953, 2018.

17) HA Hoogendoorn, W Renooij, LMA Akkermans : Long-term study of large ceramic implants (porous hydroxyapatite) in dog femora. Clin Orthop Relat Res, 187 : 281-288, 1984.

18)Merten HA, Wiltfang J, Grohmann U, Hoenig JF : Intraindividual comparative animal study of α- and β-Tricalcium phosphate degradation in conjunction with simultaneous insertion of dental implants. J Craniofac Surg, 12(1) : 59-68, 2001.

19) Kurashina K, Kurita H, Wu Q, Ohtsuka A, Kobayashi H : Ectopic osteogenesis with biphasic ceramics of hydroxyapatite and tricalcium phosphate in rabbits. Biomaterials, 23(2) : 407-412, 2002.

20) Swada K, Nakahara K, Haga-Tsujimura M, Iizuka T, Fujioka-Kobayashi M, Igarashi K, Saulacic N : Comparison of three block bone substitutes for bone regeneration: long-term observation in the beagle dog. Odontology, 106(4) : 398-407, 2018.

21) Kamakura S, Sasano Y, Shimizu T, Hatori K, Suzuki O, Kagayama M, Motegi K : Implanted octacalcium phosphate is more resorbable than beta-tricalcium phosphate and hydroxyapatite. J Biomed Mater Res, 59(1) : 29-34, 2002.

22) Weiner S, Wagner HD : The material bone: Structure mechanical function relations. Annu Rev Mater Sci, 28 : 271–298, 1998.

23) Wang Y, Azaïs T, Robin M, et al : The predominant role of collagen in the nucleation, growth, structure and orientation of bone apatite. Nat Mater, 11(8) : 724-733, 2012.

24) Kim HM, Kim YS, Woo KM, Park SJ, Rey C, Kim Y, Kim JK, Ko JS : Dissolution of poorly crystalline apatite crystals by osteoclasts determined on artificial thin - film apatite. J Biomed Mater Res, 56(2) : 250-256, 2001.

25) Loszach M, Gitzhofer F : Induction Suspension Plasma Sprayed Biological-like Hydroxyapatite Coatings. J Biomater Appl, 29(9) : 1256−1271, 2015.

26) Levingstone TJ, Ardhaoui M, Benyounis K, Looney L, Stokes JT : Plasma sprayed hydroxyapatite coatings: Understanding process relationships using design of experiment analysis. Surf Coat Technol, 283 : 29-36, 2015.

27) Nishikawa H, Hasegawa T, Miyake A, Tashiro Y, Hashimoto Y, Blank DHA, Rijnders G : Relationship between the Ca/P ratio of hydroxyapatite thin films and the spatial energy distribution of the ablation laser in pulsed laser deposition. Mater Lett, 165 : 95-98, 2016.

28) Rau JV, Cacciotti I, Laureti S, Fosca M, Varvaro G, Latini A : Bioactive nanostructured Si-substituted hydroxyapatite coatings on titanium prepared by pulsed laser deposition. J Biomed Mater Res Part B Appl Biomater, 103 : 1621-1631, 2015.

29) Ivanova AA, Surmeneva MA, Surmenev RA, Depla D : Influence of deposition conditions on the composition, texture and microstructure of RF-magnetron sputter-deposited hydroxyapatite thin films. Thin Solid Films, 591 part B : 368-374, 2015.

30) Nathanael AJ, Yuvakkumar R, Hong SI, Oh TH : Novel zirconium nitride and hydroxyapatite nanocomposite coating: Detailed analysis and functional properties.

ACS Appl Mater Interfaces, 6 : 9850-9857, 2014.

31) Oyane A, Wang X, Sogo Y, Ito A, Tsurushima H : Calcium phosphate composite layers for surface-mediated gene transfer. Acta Biomater, 8(6) : 2034-2046, 2012.

32) Oyane A, Uchida M, Choong C, Triffitt J, Jones J, Ito A : Simple surface modification of poly (ε-caprolactone) for apatite deposition from simulated body fluid. Biomaterials, 26(15) : 2407-2413, 2005.

33) Yokoyama Y, Oyane A, Ito A : Preparation of a bonelike apatite–polymer fiber composite using a simple biomimetic process. J Biomed Mater Res Part B Appl Biomater, 86(2) : 341-352, 2008.

34) Suzuki Y, Oyane A, Ikeno F, Lyons JK, Yeung AC : Development of animal model for calcified chronic total occlusion. Catheter Cardiovas Interv, 74(3) : 468-475, 2009.

35) Nathanael A. J., Oyane A, Nakamura M, Sakamaki I, Nishida E, Kanemoto Y, Miyaji H : In vitro and in vivo analysis of mineralized collagen-based sponges prepared by a plasma- and precursor-assisted biomimetic process. ACS Appl Mater Interfaces, 9(27) : 22185-22194, 2017.

36) Gu Y, Bai Y, Zhang D : Osteogenic stimulation of human dental pulp stem cells with a novel gelatin - hydroxyapatite - tricalcium phosphate scaffold. J Biomed Mater Res A, 106(7) : 1851-1861, 2018.

37) Pfaffl MW : A new mathematical model for relative quantification in real-time RT-PCR. Nucleic Acids Res, 29(9) : e45, 2001.

38) Schmittgen TD, Zakrajsek BA : Effect of experimental treatment on housekeeping gene expression: validation by real-time, quantitative RT-PCR. J Biochem Biophys Methods, 46(1-2) : 69-81, 2000.

39) Guarino V, Causa F, Netti PA, Ciapetti G, Pagani S, Martini D, Baldini N, Ambrosio

L : The role of hydroxyapatite as solid signal on performance of PCL porous scaffolds for bone tissue regeneration. J Biomed Mater Res Part B Appl Biomater, 86 : 548-557, 2008.

40) Kim SH, Oh SA, Lee WK, Shin US, Kim HW : Poly(lactic acid) porous scaffold with calcium phosphate mineralized surface and bone marrow mesenchymal stem cell. Mater Sci Eng C, 31(3) : 612-619, 2011.

41) Maeno S, Niki Y, Matsumoto H, Morioka H, Yatabe T, Funayama A, Toyama Y, Taguchi T, Tanaka J : The effect of calcium ion concentration on osteoblast viability, proliferation and differentiation in monolayer and 3D culture. Biomaterials, 26(23) : 4847-4855, 2005.

42) Lee MN, Hwang HS, Oh SH, Roshanzadeh A, Kim JW, Song JH, Kim ES, Koh JT : Elevated extracellular calcium ions promote proliferation and migration of mesenchymal stem cells via increasing osteopontin expression. Exp Mol Med, 50(11) : 142, 2018.

43) Vincent K, Durrant MC : A structural and functional model for human bone sialoprotein. J Mol Graph Model, 39 : 108-117, 2013.

44) Weinreb M, Shinar D, Rodan GA : Different pattern of alkaline phosphatase, osteopontin, and osteocalcin expression in developing rat bone visualized by in situ hybridization. J Bone Miner Res, 5(8) : 831-842, 1990.

45) Mantovani A, Biswas SK, Galdiero MR, Sica A, Locati M : Macrophage plasticity and polarization in tissue repair and remodeling. J Pathol, 229(2) : 176-185, 2013.

46) Chen Z, Mao X, Tan L, Friis T, Wu C, Crawford R, Xiao Y : Osteoimmunomodulatory properties of magnesium scaffolds coated with β-tricalcium phosphate. Biomaterials, 35(30) : 8553-8565, 2014.

47) Wang M, Yu Y, Dai K, Ma Z, Liu Y, Wang J, Liu C : Improved osteogenesis and angiogenesis of magnesium-doped calcium phosphate cement via macrophage immunomodulation. Biomater Sci, 18(11) : 1574-1583, 2016.

48) Sugimoto T, Kanatani M, Kano J, Kaji H, Tsukamoto T, Yamaguchi T, Fukase M, Chihara K : Effects of high calcium concentration on the functions and interactions of osteoblastic cells and monocytes and on the formation of osteoclast-like cells. J Bone Miner Res, 8(12) : 1445-1452, 1993.

49) Webb K, Hlady V, Tresco PA : Relative importance of surface wettability and charged functional groups on NIH 3T3 fibroblast attachment, spreading, and cytoskeletal organization. J Biomed Mater Res, 41(3) : 422-430, 1998.

50) Feller L, Jadwat Y, Khammissa RA, Meyerov R, Schechter I, Lemmer J : Cellular responses evoked by different surface characteristics of intraosseous titanium implants. Biomed Res Int, 2015 : 171945, 2015.

51) Roozbahani M, Alehosseini M, Kharaziha M, Emadi R : Nano calcium phosphate bone cement based on Si-stabilized α-tricalcium phosphate with improved mechanical properties. Mater Sci Eng C Mater Biol Appl, 81 : 532-541, 2017.

52) : Espanol M, Casals I, Lamtahri S, Valderas MT, Ginebra MP : Assessment of protein entrapment in hydroxyapatite scaffolds by Size exclusion chromatography. Biointerphases, 7(1-4) : 37, 2012.

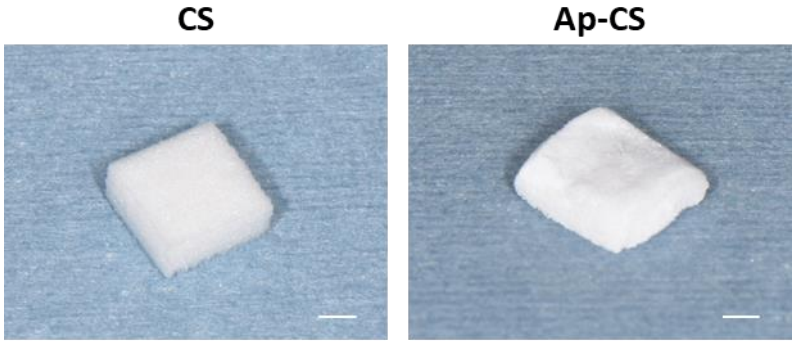


**Fig. 1**

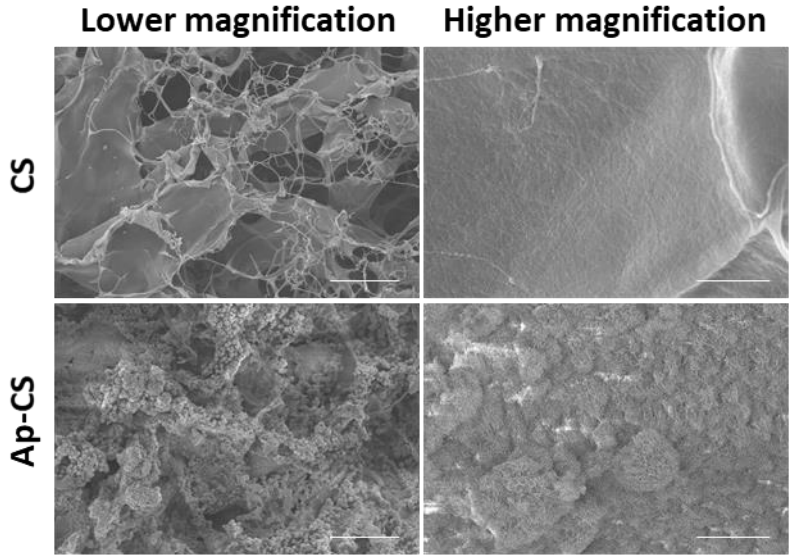


**Fig. 2**

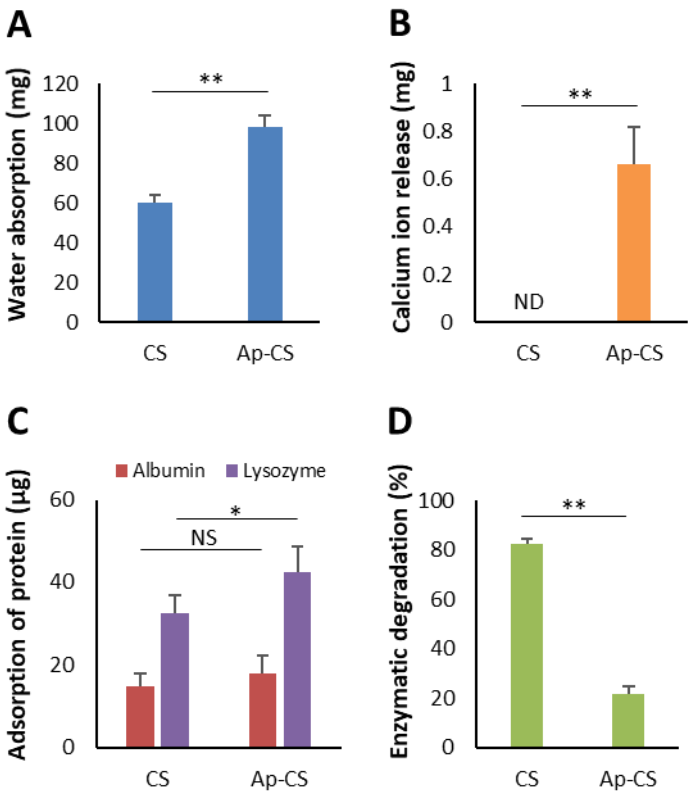
A
Water absorption (mg)
120
100
80
60
40
20
0
**
CS
Ap-CS
B
Calcium ion release (mg)
1
0.8
0.6
0.4
0.2
0
**
ND
CS
Ap-CS
C
Albumin
Lysozyme
Adsorption of protein (μg)
60
40
20
0
*
NS
CS
Ap-CS
D
Enzymatic degradation (%)
100
80
60
40
20
0
**
CS
Ap-CS

**Fig. 3**

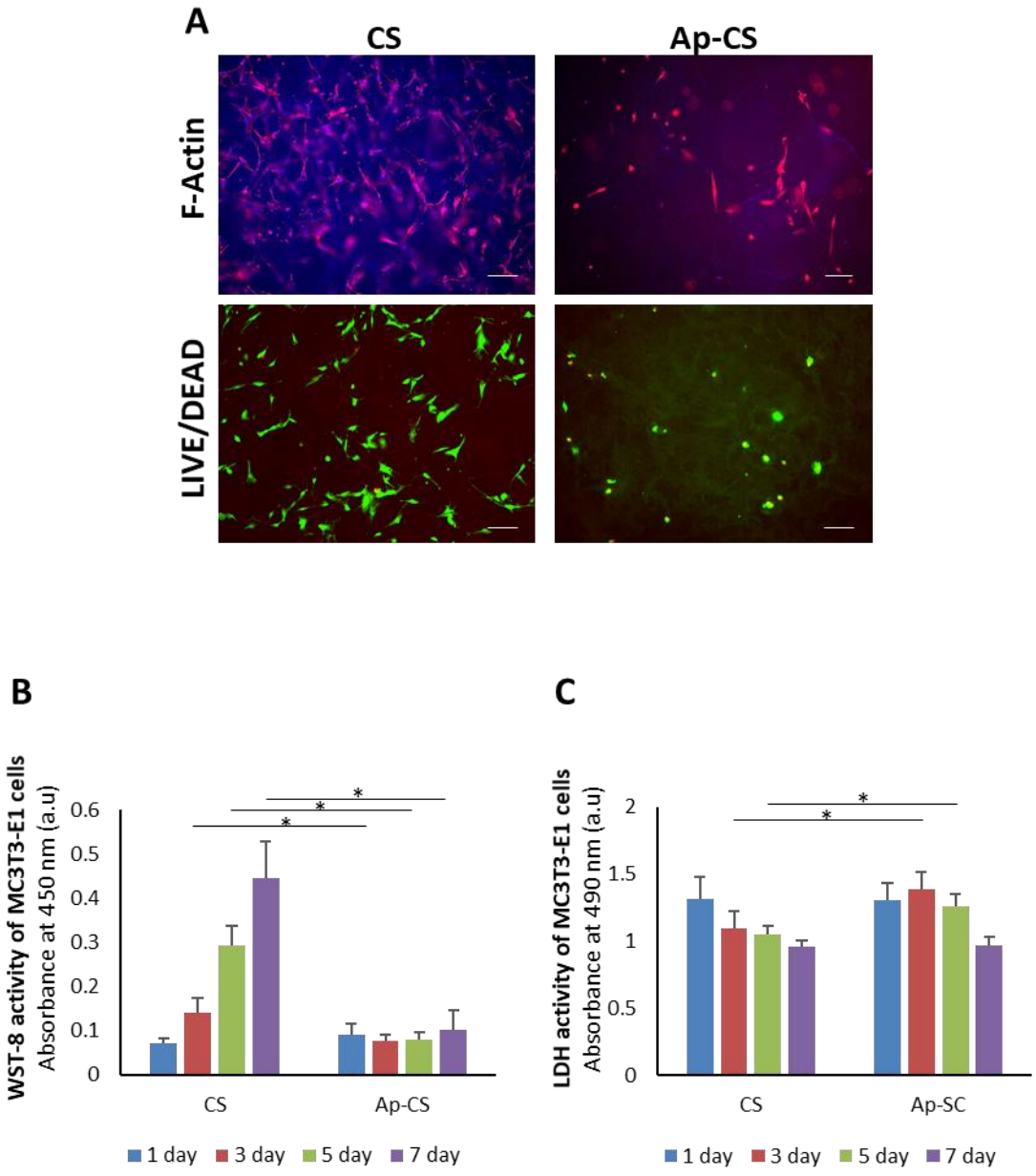
A
CS
Ap-CS
F-Actin
LIVE/DEAD
B
WST-8 activity of MC3T3-E1 cells
Absorbance at 450 nm (a.u)
0.6
0.5
0.4
0.3
0.2
0.1
0
*
*
*
CS
Ap-CS
1 day
3 day
5 day
7 day
C
LDH activity of MC3T3-E1 cells
Absorbance at 490 nm (a.u)
2
1.5
1
0.5
0
*
*
CS
Ap-SC
1 day
3 day
5 day
7 day

**Fig. 4**

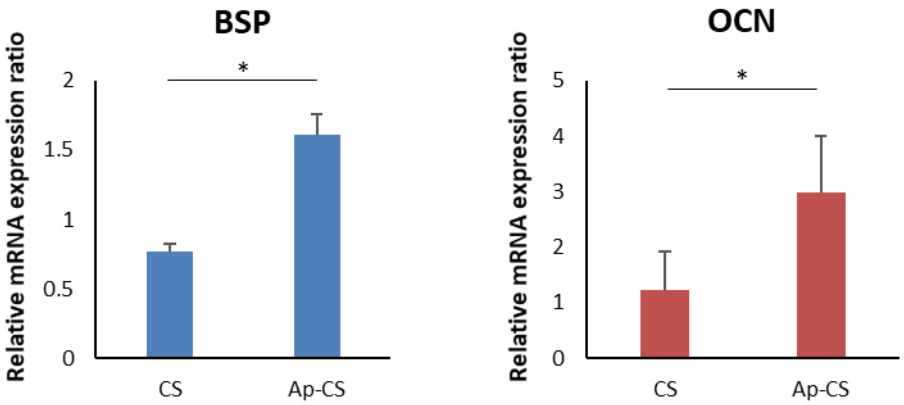
BSP
Relative mRNA expression ratio
2
1.5
1
0.5
0
*
CS
Ap-CS
OCN
Relative mRNA expression ratio
5
4
3
2
1
0
*
CS
Ap-CS

**Fig. 5**

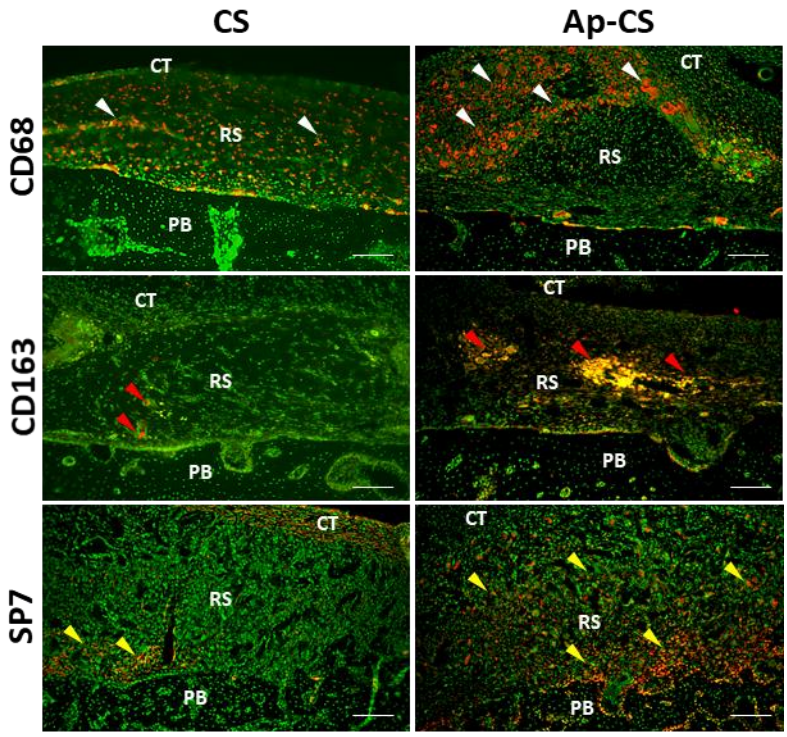


**Fig. 6**

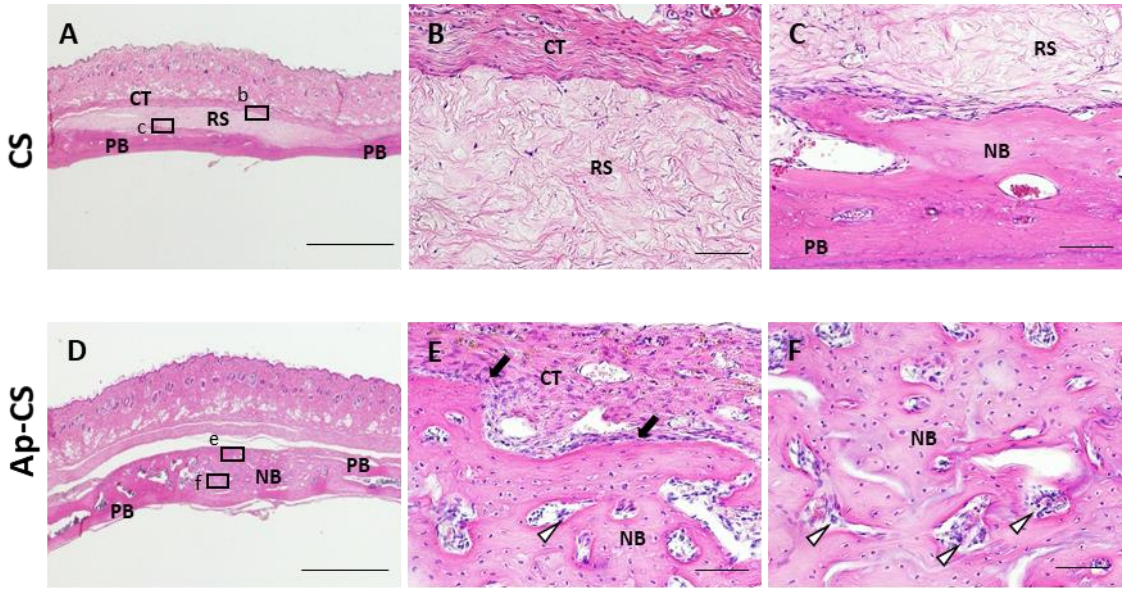


**Fig. 7**

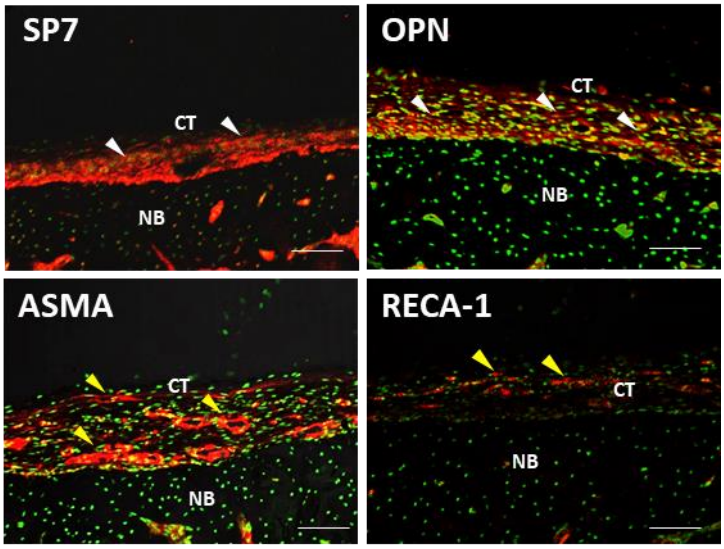


**Fig. 8**

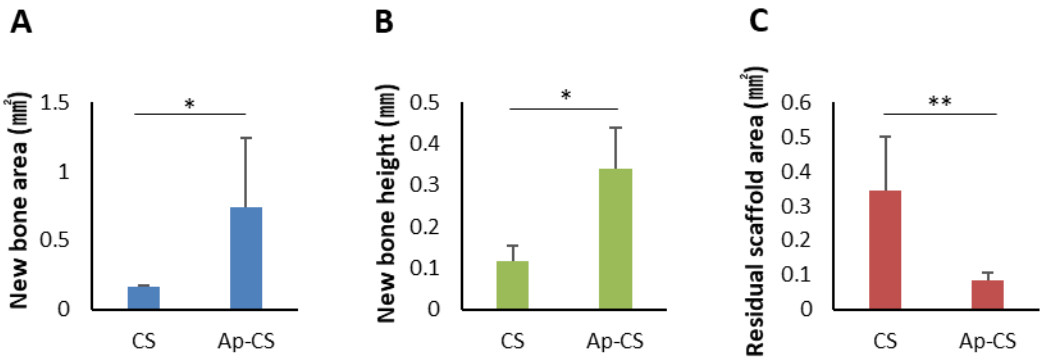
A
New bone area (㎟)
1.5
1
0.5
0
*
CS
Ap-CS
B
New bone height (㎜)
0.5
0.4
0.3
0.2
0.1
0
*
CS
Ap-CS
C
Residual scaffold area (㎟)
0.6
0.5
0.4
0.3
0.2
0.1
0
**
CS
Ap-CS

**Fig.9**

**Figure legends**

**Figure 1 Digital photograph of scaffold**

Scale bar represents 2 mm. Abbreviations: Ap-CS, apatite-coated collagen scaffold; CS, collagen scaffold.

**Figure 2 SEM images of scaffold**

Scale bar represents 100 μm in lower magnification and 5 μm in higher magnification. Abbreviations: Ap-CS, apatite coated collagen scaffold; CS, collagen scaffold; SEM, scanning electron microscope.

**Figure 3 Characterization of scaffold (n=6, mean± standard deviation)**

(A) Evaluation of water absorption, (B) calcium ion release, (C) adsorption of protein, and (D) enzymatic degradation for each scaffold. *: $P<0.05$, **: $P<0.01$. Abbreviations: Ap-CS, apatite-coated collagen scaffold; CS, collagen scaffold; ND, not detected, NS; Not significant.

**Figure 4 Assessments of cytocompatibility of scaffold**

(A) F-actin and LIVE/DEAD BacLight staining of MC3T3-E1 cells after 24 h of incubation. Scale bar represents 100 μm. (B) WST-8 activity of MC3T3-E1 cells (n=5, mean ± standard deviation). *: $P<0.05$. (C) LDH activity of MC3T3-E1 cells (n=5, mean ± standard deviation). *: $P<0.05$. Abbreviations: Ap-CS, apatite-coated collagen scaffold; CS, collagen scaffold; LDH, lactate dehydrogenase; WST-8, water-soluble tetrazolium salts-8.

**Figure 5 RT-PCR assessments (n=3, mean ± standard deviation)**

Measurements of amplified cDNA of BSP and OCN. *: $P<0.05$. Abbreviations: Ap-CS, apatite coated collagen scaffold; BSP, bone sialoprotein; CS, collagen scaffold; OCN, osteocalcin; RT-PCR, reverse transcription polymerase chain reaction.

**Figure 6 Immunohistochemical observation of scaffold at 10 days after implantation**

The targets and nuclei are stained in red and green, respectively. Scale bar represents 100 μm. Abbreviations: Ap-CS, apatite-coated collagen scaffold; CS, collagen scaffold; CT, connective tissue; PB, pre-existing bone; RS, residual scaffold

**Figure 7 Histological findings at 35 days after implantation of scaffold**

(B), (C) and (E), (F) present higher magnification of the framed areas in (A) and (D), respectively. Scale bar represents 2 mm (A, D) and 100 μm (B, C, E, F). Staining: hematoxylin-eosin. Abbreviations: Ap-CS, apatite-coated collagen scaffold; CS, collagen scaffold; CT, connective tissue; NB, new bone; PB, pre-existing bone; RS, residual scaffold.

**Figure 8 Immunohistochemical observation of Ap-CS at 35 days after implantation**

The targets and nuclei are stained in red and green, respectively. Scale bar represents 100 μm. Abbreviations: Ap-CS, apatite-coated collagen scaffold; ASMA, α-smooth muscle actin; CT, connective tissue; NB, new bone; OPN, osteopontin; RECA-1, rat endothelial cell antigen-1.

**Figure 9 Histomorphometric measurements (n=5, mean ± standard deviation)**

(A) bone area, (B) bone height and (C) residual scaffold area. *: $P<0.05$, **: $P<0.01$.

Abbreviations: Ap-CS, apatite-coated collagen scaffold; CS, collagen scaffold.